# Stator Design and Air Gap Optimization of High Speed Drag-Cup Induction Motor using FEM

Mladen V. TERZIC, Dragan S. MIHIC, Slobodan N. VUKOSAVIC
*Faculty of Electrical Engineering, University of Belgrade, 11000 Belgrade, Serbia*
*terzic@etf.rs, dragan84m@etf.rs, boban@etf.rs*

***Abstract*—A huge number of modern applications nowadays require the use of high speed electrical machines which need to be highly optimized in order to achieve the best efficiency and the lowest mass and price. The low rotor inertia is also an important requirement in order to reduce rotor kinetic energy. The subject of this paper is high speed drag-cup induction motor (IM) with low inertia which is designed for use as an auxiliary motor in automotive systems such as Kinetic Energy Recovery System (KERS) in Formula 1. This work presents the procedure for stator design and optimization of the air gap length and rotor thickness of this kind of motor in order to achieve the highest efficiency in the speed range of interest. Simple procedure for stator dimensioning was developed and it was shown how the optimal number of stator conductors could be calculated. The effect of change in rotor thickness and air gap lengths on motor performance is demonstrated through some analytical considerations. The machine is then modeled in FEM software by means of which the optimization of the air gap and rotor thickness was performed. At the end, the simulation results were presented and analyzed and conclusions were drawn.**

***Index Terms*—finite element methods, induction motor, high speed machines, low inertia, optimization.**

## I. Introduction

Many new electrical machine applications in automotive and distributed resource systems, such as electrical generators and motors, micro-turbines etc., put very high demands to their design [1-4]. Low-cost and light weight machines with very high efficiency are preferable. During the past few years, high speed motors have become more popular because of their high specific power (W/kg). Beside aforementioned applications, high speed motors are widely used in industrial applications such as compressors, drills, pumps etc., in which they bring more simplicity to the system because of gears absence. Numerous machines were designed and optimized for utilization in these applications in a wide speed range from 10krpm to 100krpm [5-7]. Low rotor inertia is also desirable in order to reduce rotating system kinetic energy. This brings safety to the environment and guarantees a significant reduction of mechanical vibrations, due to mass decrease and potential sources of rotor imbalance. In addition to this, starting and reversing times of motor have been significantly reduced.

All machine types can be found in high speed applications. Induction motors (IM) are dominant in middle and high power and speed range as reported in [8], because of their mechanical robustness and simple construction. Various kinds of induction motors are designed for high speed applications such as: squirrel cage IM [9], solid rotor IM [10-11], copper coated solid rotor IM [12] etc. Different rotor structures are compared in [13] all of them having relatively high inertia of the rotor.

The idea for reducing of rotor inertia was introduced in [14] where different rotor structures had been designed. Drag-cup rotor was first introduced in [15] where its parameters were analytically developed. This kind of rotor is the result of desire to split torque producing part in the form of the copper alloy cup from the heavily rotor magnetic circuit. Motor with this kind of rotor for high speed turbo molecular pump application was developed in [16]. The problem of this type of IM is relatively poor efficiency because of high losses in the rotor cup. Also, this motor has a low power factor due to large air gap which consists of two air gaps and the cup. This gives rise to stator copper loses due to higher magnetizing current. However, good solutions may be achieved by careful design of all parts of drag-cup motor, especially rotor and air gap, as outlined in [16].

The subject of this paper is the design of high speed IM which is intended for use in an auxiliary system of the car such as KERS. The approximate values of input parameters were found in [3] where SMPM was designed for use in Formula 1 KERS. Simple stator design procedure was developed using main analytical formulas and some specificity of high speed machines found in reference literature. It was shown then, through some analytical considerations, how cup thickness and air gap lengths affects motor performance. Rough boundary values for these parameters were also obtained as a result of this analysis. After this, whole machine was modeled in FEM software where optimization of the rotor thickness and air-gap length was performed by series of simulations. The aim was to find the best solution with regard to motor efficiency.

## II. Stator Dimensioning

The stator design has been simplified and so it doesn't include some aspects such as thermal and mechanical. Detailed optimization was left for the future studies. Input design parameters are summarized in Table I. They are taken from the reference KERS PMSM design that is developed in [3].

### A. Stator winding design

In the case of high speed IM it is very important to have a smooth sinusoidal air gap flux at the surface of the rotor, otherwise, the harmonic components will induce a large amount of losses on the rotor surface [17]. This can be achieved by making the stator magnetomotive force (mmf) as sinusoidal as possible. It was shown in [18], that the use

Digital Object Identifier 10.4316/AECE.2013.03015

of a larger number of stator slots and also two layer chorded stator winding can significantly reduce harmonic content in stator mmf.

TABLE I. INPUT PARAMETERS OF THE MOTOR

| Input Parameters | Values |
|---|---|
| Rated power $P_n$ [kW] | 50 |
| Synchronous speed $n_s$ [rpm] | 24000 |
| Number of phases $m$ | 3 |
| Rated phase voltage $U_n$ [V] | 400 |
| Phase connection | D |
| Rated phase current $I_n$ [A] | 62,4 |
| Pole pairs $p$ | 2 |
| Stator frequency $f$ [Hz] | 800 |
| Rated power factor $cos\varphi_n$ | 0,74 |
| Rated efficiency $\eta$ [%] | 90,00 |

Cording factor is defined as [19]:

$$c_f = \frac{W}{\tau_s} \tag{1}$$

where $W$ is the coil span and $\tau_s$ is the pole pitch.

The harmonic content of stator's mmf can be approximately predicted by the leakage factor [19]:

$$\sigma = \sum_{\nu \neq 1} \left( \frac{\xi_\nu}{\nu \xi_1} \right)^2 \tag{2}$$

Where $\nu$ is the harmonic order, $\xi_\nu$ is the winding factor of $\nu^{th}$ harmonic and $\xi_1$ is the winding factor of fundamental (first) harmonic. The smaller leakage factor means fewer harmonics in the stator's mmf. Leakage and winding factors for the first harmonic and two numbers of stator slots and chording factors are calculated and summarized in Table II.

According to Table II, two layer chorded stator winding with $Q = 36$ slots was selected. Perhaps, the only drawback of two-layer winding is the decrease of the slot-filling factor due to main voltage insulation required between two phases in the same slot. Also, the winding factor of the fundamental mmf is slightly reduced. However, these drawbacks are not as serious as benefits that are gained by the reduction of mmf harmonics.

TABLE II. LEAKAGE AND WINDING FACTORS FOR DIFFERENT NUMBER OF STATOR SLOTS AND CHORDING FACTOR

| Number of stator slots $Q$ and chording factor $c_f$ | Winding factor $\xi_1$ | Leakage factor $\sigma$ |
|---|---|---|
| Q = 24, $c_f$ = 1 | 0.9659 | 0.1016 |
| Q = 24, $c_f$ = 5/6 | 0.9330 | 0.0627 |
| Q = 36, $c_f$ = 1 | 0.9598 | 0.0745 |
| Q = 36, $c_f$ = 5/6 | *0.9452* | *0.0568* |

Furthermore, cross section of stator wire and winding must be determined. First, rated phase current has to be calculated using the values of rated power, voltage, power factor and coefficient of efficiency from Table I. The calculated value is given in Table I.

Allowed current densities for different cooling systems of high speed machines and maximal temperature of stator conductors of 250°C are summarized in [20]. Motors for KERS are commonly cooled by circulation of gearshift oil [3]. Taking this into consideration and according to the table of allowed current densities for different cooling systems given in [20] the current density $J$ of 10 A/mm$^2$ was selected. Using this value, cross section of one conductor $S_{Cu1}$ can be calculated. Wire diameter can be calculated from the value of cross section. It must be mentioned here that stator wire is stranded in order to reduce the skin effect and to avoid its calculation. Also, it is presumed that standard transposition of conductors is performed so that the proximity effect can also be neglected in the calculations.

### *B. Determination of optimal number of phase conductors and main stator dimensions*

Now, the approximate cross section occupied by conductors in one stator slot $S_{Cusl}$ can be expressed as a function of the number of phase conductors $N_p$:

$$S_{Cusl} = N_{sl} S_{Cu1} = \left( N_p \frac{m}{Q} \right) S_{Cu1} \tag{3}$$

where $N_{sl}$ is the number of conductors per slot. Formula (3) will be used later on for the determination of optimal number of phase conductors.

To find the optimal value for number of stator's phase conductors another formula for a cross section of conductors in one slot must be derived and it must be a function of main stator dimensions and number of phase conductors. It can be shown using the basic IM formulas found in [21] that cross section of stator slot conductors can be connected with main stator parameters with the following formula:

$$S_{Cusl} = \frac{5,3 U_{pn}}{Q^2 f N_p \xi_1 B_{m\delta}} \tag{4}$$

Values calculated by (3) and (4) must be equal. If (3) and (4) are plotted as functions of $N_p$, the point of their intersection represents the value of $N_p$ that fulfills all input parameters and design requirements. Optimal value is found to be 112. Using this value, number of conductors per slot is calculated and it is found to be 9. Considering that this number must be even in the case of two-layer winding, the value of 8 is taken. With an adopted number of conductors per slot, all stator parameters are recalculated and presented in Table III.

It is only left to calculate the yoke width $h_y$ and the outer diameter of the stator $D_{so}$. The yoke width is calculated with the aim to limit its magnetic induction $B_{my}$ to about 1 T. Because flux per pole splits into two equal parts and then travels stator back iron, width of back iron can be calculated as:

$$h_y = \frac{B_{m\delta} \tau_s}{2 B_{my} l_s} \tag{5}$$

Somewhat higher value than calculated was adopted because stator back iron must have enough space for axial cooling channels in the final design. Moreover, when all geometry values are known, $D_{so}$ is simply calculated and its value is presented in Table III along with yoke width.

Geometry of designed stator is shown in Fig. 1. Only one quarter of machine i.e. one pole was shown because of symmetry. The enlarged detail in Fig. 1 displays stator's slot geometry.

## III. Analytical Considerations of Rotor Thickness and Air Gap Lengths Impact on Motor Performance

Very important part of drag-cup IM is its air gap. It affects many machine parameters such as: no load current, stator leakage inductance, brake-down torque and copper losses. Total air gap of drag-cup IM consists of three parts: inner air gap of length $d_1$, rotor cup with thickness $d_c$ and outer air gap of length $d_2$. All parts of total air gap are shown by enlarged detail in Fig. 2. The main result of the following analysis will be the approximate boundary values for all parts of the total air gap which will be used in the optimization process later on. Also, it will be shown that there is a need for optimization of these geometry parameters which will lead to design providing the best possible efficiency. A series of assumptions is made including an infinite iron permeability and sinusoidal distribution of the air gap induction.

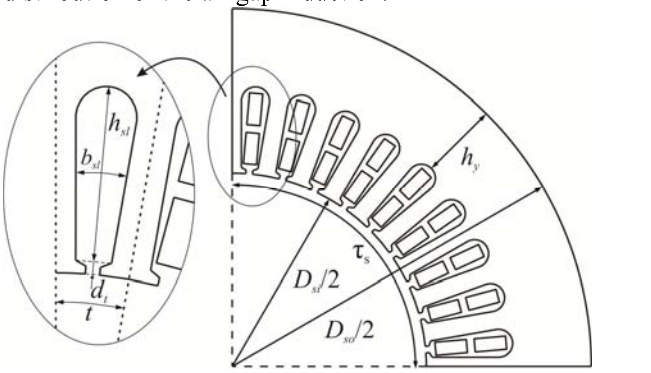


Figure 1. Geometry of designed stator and stator slot with main dimensions whose values are given in Table III

TABLE III. STATOR PARAMETERS AND GEOMETRY DATA

| Parameters | Values |
|---|---|
| Number of slot conductors $N_{sl}$ | 8 |
| Number of phase conductors $N_f$ | 96 |
| Pole pitch $\tau_s$ [mm] | 68 |
| Slot pitch $t$ [mm] | 7,5 |
| Slot width $b_{sl}$ [mm] | 5 |
| Slot height $h_{sl}$ [mm] | 25 |
| Stack length $l_s$ [mm] | 102 |
| Inner diameter $D_{si}$ [mm] | 86,5 |
| Yoke height $h_y$ [mm] | 30 |
| Outer diameter $D_{so}$ [mm] | 196,5 |

The increase of total air gap gives rise to the no load or magnetizing current of the motor. It can be shown that the percent value of no load current $i_0$ of the IM can be related to the total air gap length with the following equation:

$$i_0 = \frac{6\sqrt{2} B_{m\delta}\delta}{\mu_0 \pi N_f I_n} \cdot 100 \tag{6}$$

where $\delta$ is the total air gap length and $\mu_0$ is the magnetic permeability of vacuum. Equation (6) was derived from the basic IM equations taken from [22].

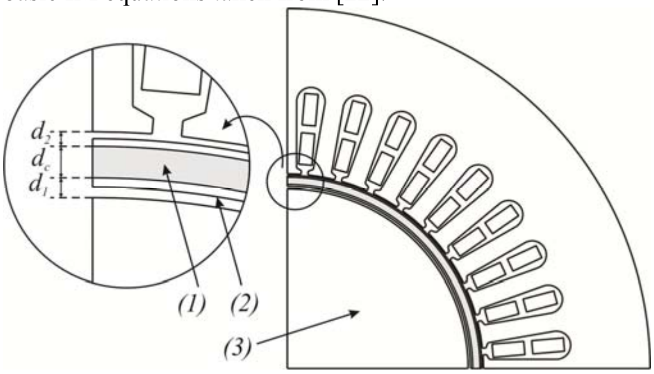


Figure 2. Quarter of 2D motor geometry with detail of drag-cup rotor and air gaps: (1) – drag-cup rotor; (2) – band which defines rotational parts; (3) – rotor magnetic circuit; $d_c$ – drag-cup thickness; $d_1$, $d_2$ – inner and outer air gap, respectively.

The maximum value of no load current is about 40% of nominal phase current for standard induction motors. Naturally, drag-cup IM has the larger air gap in such a way that the value of 70% can be taken as an acceptable maximum value. Because all values from equation (6) are known, maximal permissible air gap was determined and found to be 5.6 mm. Larger values can unnecessarily increase the stator copper losses and decrease the motor efficiency. Power factor also decrease because motor needs more reactive energy for magnetization.

Increase of total air-gap length also affects the stator leakage inductance. The part of it, which is called tooth tip inductance $L_d$ and which is the most affected by increase of total air gap, is presented by the following equation [19]:

$$L_d = \frac{m}{Q}\mu_0 l_s N_f^2 k_2 \frac{5\left(\frac{\delta}{b_1}\right)}{5+4\left(\frac{\delta}{b_1}\right)} \tag{7}$$

where $b_1$ is the width of the slot opening and $k_2$ is constant which is calculated by the formula given in [19]. Increased leakage inductance produces smaller brake down torque $T_b$ as can be seen from the following formula [22]:

$$T_b = \frac{3p}{2L_{\gamma e}}\frac{U_n^2}{\omega_s^2} \tag{8}$$

where $L_{\gamma e}$ is the equivalent leakage inductance which approximately equals the sum of stator and rotor leakage inductances and $\omega_s$ is the synchronous electrical angular speed of the motor. Decrease of brake down torque is another reason why equivalent air gap cannot be increased to much. FEM simulations will also show this phenomenon.

Losses in the rotor cup are relatively large and that is one of the problems of the drag-cup IM as stated before. These losses are inversely proportional to rotor thickness as can be seen from the analytical formula that was derived in [15]. Thus, by increasing the cup thickness, motor efficiency grows but only to the certain point at which the negative consequences of increased total air gap prevail and cancel the benefits of smaller cup losses. This is mostly due to the fact that large air gap increases stator copper losses as it was stated before. This analysis shows that there is an optimal value for rotor cup thickness.

Losses in the drag-cup also depend on the harmonic content of the stator's mmf as it was asserted before. It was shown in [23] that increasing the distance between rotor and stator surfaces, i.e. air gap $d_2$, attenuates the higher harmonics of stator's mmf and in that way additional losses in the cup decrease. This, of course, increases the motor efficiency. But, similarly like for the rotor thickness, above the certain value of $d_2$ negative consequences of increased total air gap prevails the benefits of smaller additional rotor losses. Motor efficiency starts to fall from that value of outer air gap thickness. This shows that an optimal value for outer air gap thickness can also be found.

As for the inner air gap concerns, its increasing lowers the magnetic coupling between rotor and stator and has no benefits on motor efficiency, so it is good to keep it as small as possible to decrease the total air gap length. Because of this, there is no need to take into account inner air gap change in the optimization process.

Maximum allowed clearance between stationary and rotational parts limits the minimal values of both inner and outer air gaps to about 1 mm. This is mostly due to the fact that copper alloy and iron have different thermal expansion coefficients. Minimal value for the rotor thickness is taken to be 1.5 mm because of mechanical reasons. Mechanical stresses are higher when rotor is thinner, especially at high rotational speeds and high torques. Detailed analysis of these mechanical and thermal aspects is out of scope of this work and will be the subject of the future authors' work.

All determined boundary values for the drag-cup thickness and air gaps lengths are summarized in Table IV. It must be mentioned that in optimization process only one parameter will be increased at the time, while others are kept constant. Also, it must be taken into consideration that total air gap must be less or equal to 5. 6 mm in the final design. Detailed optimization plan will be given later on.

TABLE IV. BOUNDARY VALUES FOR ROTOR THICKNESS AND AIR GAPS LENGTHS

| Parameters | Min [mm] | Max [mm] |
|---|---|---|
| $d_1$ | 1 | 1 |
| $d_2$ | 1 | 3.76 |
| $d_c$ | 1.5 | 3.12 |
| $\delta_e$ | 3.5 | 5.6 |

## IV. FEM Modeling Of Drag-Cup IM

There are some common steps that must be performed in 2D FEM modeling process of the motor. The most important steps will be explained in this chapter.

### A. *Geometry, boundaries, mesh and torque definitions*

Previously determined stator geometry with the data given in Table III and drag-cup rotor geometry were drawn in 2D and presented in Fig. 2. Because of symmetry, only one pole of motor i.e. a quarter of motor cross section was modeled. In order to account for symmetry, the periodical boundary condition was applied to the left and right boundaries of the motor [24]. Zero magnetic potential boundary condition was applied to the outer boundary of the motor [24].

Mesh is defined to every part of the motor separately. It is the most important to have a good mesh in air gap region to ensure precise calculation of the motor torque and cup losses. In this model the minimum size of the mesh element in the air gap region was set to 0, 2 mm to ensure that in every case there will be at least two layers of mesh in each part of the total air gap. Sliding mesh was applied to drag-cup as the only moving part of the motor and it was defined by band region that is shown in Fig. 2.

After the mesh is defined, in every nod the following partial differential equation is applied:

$$\nabla \times \frac{1}{\mu} \cdot \nabla \times A = J_s - \sigma \frac{\partial A}{\partial t} - \sigma \cdot \nabla V + \sigma v \times \nabla \times A \quad (9)$$

where $A$ is the magnetic vector potential, $v$ is the speed of moving parts, $V$ is the electric potential, $\mu$ and $\sigma$ are the permittivity and conductivity of material respectively and $J_s$ is the current density of current sources. Having solved the system of these equations, distribution of magnetic induction and current density is made available. Distribution of magnetic induction and flux lines for one solution in one time instant are shown in Fig. 3.

Torque $T$ that acts on the cup was calculated by the following equation that represents the Lorentz torque:

$$T = \int_{V_c} \vec{r} \times \left( \vec{J}(t) \times \vec{B}(t) \right) dV_c \quad (10)$$

where $r$ is the displacement vector from the axis of rotation, *J(t)* is the current density vector of induced currents in the cup and *B(t)* is the magnetic induction vector, $dV_c$ is the volume of one element and $V_c$ is total volume of the drag-cup.

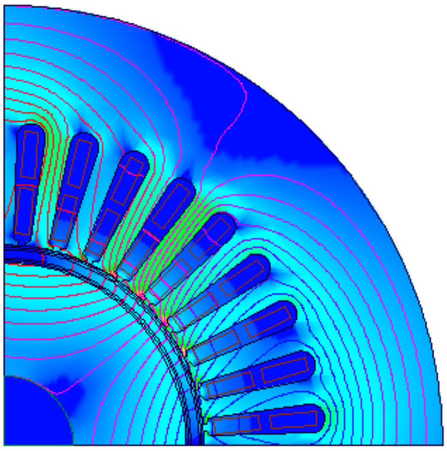

Figure 3. Field distribution in motor in for one combination of rotor parameters in one time instant

### B. *Assignment of material properties and calculation of losses*

Stator conductors were defined as stranded copper wires and because there are lots of strands in a single wire, skin effect was neglected in calculations of stator copper losses, as mentioned before. It is also presumed that standard transposition of conductors was performed so the proximity effect was also neglected in the calculations. According to all these assumptions stator copper losses $P_{Cus}$ are calculated by the following equation:

$$P_{Cu,s} = 3 R_{DC} I^2 \quad (11)$$

where $R_{DC}$ is the DC resistance of one phase and $I$ is the rms value of phase current which was calculated through FEM simulations. Phase DC resistance was calculated by the standard equation using the properties of the designed winding and it is found to be 6 mΩ.

The drag-cup material was defined as solid copper. In the drag-cup, skin-effect cannot be neglected, so the drag-cup losses $P_{Cu,c}$ were calculated according to the following equation:

$$P_{Cu,c} = \frac{1}{\sigma_{Cu}} \int_{V_c} J^2 dV_c \quad (12)$$

where $\sigma_{Cu}$ is electrical conductivity of copper and $J$ is the module of induced current density, vector in one finite element.

The stator and rotor magnetic circuits are made from magnetic steel sheets for rotating machines. It is very important to choose the proper thickness of the sheet in order to minimize eddy current loss in the single sheet. Eddy current loss depends on the penetration depth which is calculated according to the following equation [19]:

$$\delta = \sqrt{\frac{1}{\pi f \mu_0 \mu_r \gamma}} \quad (13)$$

where $\delta$ is the penetration depth, $f$ is the main frequency of electromagnetic field applied to the material, $\mu_r$ is the relative permeability of the material and $\gamma$ is the electrical conductivity of the material. The frequency of 800 Hz penetration depth is 0.22 mm for the standard magnetic steel sheet conductivity and for the motor supply. Magnetic steel sheet of 0.2 mm thickness was chosen from the table of standard magnetic steel sheets for rotating machinery found in [25]. This ensures that skin effect can be neglected in the chosen sheets, because penetration depth is bigger than the actual thickness of the steel sheet. There is also proximity effect between sheets in the stack which forces the eddy currents into the sheets near the ends of the stack. There are the reasons to believe that this won't make the optimization process less effective.

The magnetic steel sheet is then defined by two main characteristics: B-H curve and specific core loss (W/kg) versus magnetic induction at one frequency. Those curves were taken from [25] for the magnetic steel sheet with the chosen thickness. The B-H curve was implemented directly in the program in the form of data table. Core losses in one element of the mesh and one time instant are calculated according to the following equations [26]:

$$p_v = \Delta l_s k_v \left( f B_m \right)^2 \tag{14}$$

$$p_h = \Delta l_s k_h f \left( B_m \right)^2 \tag{15}$$

$$p_d = \Delta l_s k_d \left( f B_m \right)^{1.5} \tag{16}$$

where $p_v$, $p_h$ and $p_d$ are eddy current, hysteresis and excess losses in one element respectively, $\Delta$ is the element area, $B_m$ is magnetic field density in the element and $k_v$, $k_h$ and $k_d$ are material constants. These constants were calculated in the following way.

Constant $k_v$ was determined from equation [26]:

$$k_v = \pi^2 \sigma \frac{d^2}{6} \tag{17}$$

where $\sigma$ and $d$ are the electrical conductivity and thickness of chosen steel sheet, respectively. They are given in Table V for the chosen steel sheet along with calculated value of $k_v$.

Data for specific core loss that are given in the table form can be interpolated using following fitting equation:

$$p_{Fe} = p_h + p_v + p_d = K_1 B_m^2 + K_2 B_m^{1,5} \tag{18}$$

where $K_1$ and $K_2$ are interpolation coefficients which can be calculated by minimizing the following error function:

$$err\left(K_1, K_2\right) = \sum_i \left[ p_{Fe,i} - \left( K_1 B_{m,i}^2 + K_2 B_{m,i}^{1.5} \right) \right]^2 = \min \tag{19}$$

where $p_{Fe,i}$ is the value of specific core loss from the defined table and for the value $B_{m,i}$ of magnetic induction. Now, from the equations (13), (14), (15) and (18), coefficients $K_1$ and $K_2$ can be related to the constants $k_v$, $k_h$ and $k_d$:

$$K_1 = k_h f + k_v f^2 \tag{20}$$

$$K_2 = k_d f^{1.5} \tag{21}$$

Using equations (17), (20) and (21) all constants were calculated and summarized in Table V in addition to other main properties of chosen steel sheet. As can be seen from Table V coefficient of eddy current loss is much smaller than hysteresis coefficient, which is the consequence of the selected sheet thickness.

After magnetic field calculation in each time step, formulas (14), (15) and (16) are used by the program in order to calculate core losses in every finite element of the mesh in the regions of the stator and rotor magnetic circuits. Total core losses in one time step were calculated by summation of losses in each finite element.

Vacuum was assigned to the rest of the model parts.

TABLE V. PARAMETERS OF MAGNETIC STEEL SHEET

| **Steel sheet - FeV 310-50-HA** | **Value** |
|---|---|
| $k_v$; $k_h$; $k_d$ | 0,132; 148,8; 1,3 |
| Thickness $d$ [mm] | 0,2 |
| Conductivity $\sigma$ [MS] | 2 |

### *C. Definition of external circuit*

Stator conductors were connected to form a double layer chorded winding that was defined in the previous chapter. Symmetrical three-phase sinusoidal voltage source was applied to the stator phases. Voltage rms value and frequency are defined in Table I. Because the motor is presented in 2D the end winding connections are not modeled. However, end connections leakage reactance is not small, especially in the case of high speed machines with small number of poles. To account for this effect in calculations, end-winding inductance $L_{ew}$ was determined using the following equation [19]:

$$L_{ew} = \frac{m}{Q} q N_f^2 \mu_0 l_w \lambda_w \tag{22}$$

where $q$ is the number of slots per pole and phase, $l_w$ is the length of the end windings and $\lambda_w$ is the permeance factor which can be taken from table in [19] for appropriate stator winding. Calculated stator leakage inductance is 0.0783 mH and it has been connected in series with the voltage supply.

### *D. Parameters of the simulation*

The rotational speed was defined as a program variable in rpm. When simulation for one speed is finished the speed is automatically changed to a new value in the range from 22000 rpm to 24000 rpm and in the steps of 200 rpm.

Simulation time was set to 220 ms and time step was set to 25 µs in order to get good resolution of calculated data. After field calculation, post processing was performed in order to calculate developed motor torque and core and copper losses in the motor as it was described before.

### *E. Air-friction loss*

In order to find motor efficiency, air-friction loss must be estimated because it cannot be calculated through the FEM simulations. It was found in [27] that the air-friction loss $P_f$ can be represented by the following formula:

$$P_f = k_r C_f \rho \pi \omega^3 R_r^4 l_r \tag{23}$$

where $k_r$ is roughness coefficient, $C_f$ is friction coefficient, $\rho$ is specific mass of air, $\omega$ is the angular velocity of the rotor, $R_r$ is the outer radius of the rotor and $l_r$ is the axial length of the rotor. Because the rotor surface is perfectly smooth, roughness coefficient is 1. Coefficient of friction can be calculated by following formula as reported by Yamada in [28]:

$$C_f = \frac{0,0152}{R_e^{0,24}}, \quad 800 < R_e < 6 \cdot 10^4 \tag{24}$$

where $R_e$ is Reynolds number which determines the type of fluid flow and for the enclosed cylinder it can be calculated as:

$$R_e = \frac{\rho \omega R_r d}{\mu_v} \tag{25}$$

where $\mu_v$ is the dynamic viscous friction of air and $d$ is the air gap thickness. Using formulas (23), (24) and (25) air-friction loss was calculated for every combination of rotor thickness and air gap lengths and for every speed in previously defined range. It must be mentioned that total air-friction loss was calculated as the sum of friction losses from both sides of the drag-cup, which are both calculated using (23).

## V. Optimization Process, Results And Discussion

Optimization process was conducted by changing the cup thickness and outer air gap length in ranges that are defined in Table IV in the following way.

First, rotor thickness was changed from 1.5 mm to 3.12 mm with 20 % of steps, while the air gap lengths were set to 1 mm and kept constant. For each combination, simulations were performed for every speed within the given range. Having completed simulation runs, the torque and power losses are calculated in the prescribed way, and the efficiency calculated as:

$$\eta = \frac{P_m}{P_m + P_\gamma} \cdot 100 \tag{26}$$

where $P_m$ is the obtained mechanical power and $P_\gamma$ is the sum of all losses in the motor:

$$P_\gamma = P_{Fe} + P_{Cu,s} + P_{Cu,c} + P_f \tag{27}$$

Power factor was found as:

$$\cos\varphi = \frac{P_m + P_\gamma}{3U_n I} \tag{28}$$

Family of characteristics that represent mechanical power versus motor speed is shown in Fig. 4 for different cup thicknesses. These characteristics were obtained by interpolating simulation results. Horizontal line in Fig. 4 represents the rated motor power and its intersections with the torque curve denote the rated speed for each cup thickness. It can be seen from Fig. 4 that brake-down torque decreases with the increase of the cup thickness, which proves the previously conducted analysis. Fig. 44 also shows that values of rated slip decrease as cup thickness grows which means that rotor losses are smaller for the same output power that was also stated in the previous analysis.

Using determined values for rated speeds, rated values for all losses and current were found by simulation data interpolation. After that, efficiency and power factor are calculated according to (26) and (28). All rated values are given in Table VI for all cup thickness values.

Values of efficiency rated coefficient, given in Table VI, are now interpolated and fitting curve is shown in Fig. 5. Fig. 5 shows that the best coefficient of efficiency is 79.47 % and that it is achieved for the rotor thickness of 1.8 mm. During further optimization process, this value of rotor thickness is taken as optimal and it was not changed.

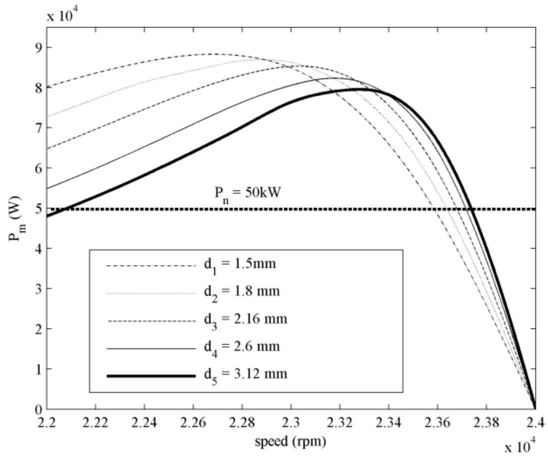


Figure 4. Mechanical characteristics for various drag-cup thicknesses

TABLE VI. RATED MOTOR PARAMETERS FOR DIFFERENT VALUES OF ROTOR THICKNESS

| $d_c$ [mm] | $n_n$ [rpm] | $I_n$ [A] | $\eta_n$ [%] | $\cos\varphi_n$ |
|---|---|---|---|---|
| 1,5 | 23500 | 71,8 | 79,10 | 0,70 |
| 1,8 | 23566 | 75,0 | 79,47 | 0,65 |
| 2,16 | 23617 | 78,9 | 79,28 | 0,61 |
| 2,6 | 23658 | 83,7 | 78,02 | 0,62 |
| 3,12 | 23687 | 89,2 | 76,39 | 0,54 |

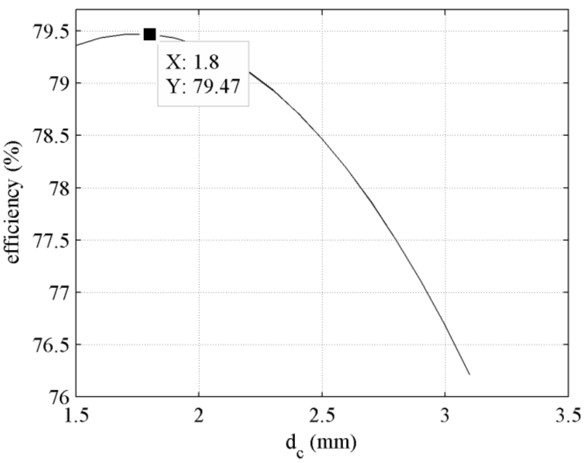


Figure 5. A curve that fits the values of efficiency rated coefficient for different values of drag-cup thickness

Next, the influence of outer air gap thickness on motor parameters was investigated. Length of outer air gap was changed from 1 mm to 3.76 mm with 20 % of steps. The same procedure for data processing was applied and calculated nominal values for speed, current, coefficient of efficiency and power factor are given in Table VII. for different values of outer air-gap length. Again, nominal values of coefficient of efficiency were interpolated and fitting curve is presented in Fig. 6.

TABLE VII. RATED MOTOR PARAMETERS FOR DIFFERENT VALUES OF OUTER AIR GAP LENGTH

| $d_2$ [mm] | $n_n$ [rpm] | $I_n$ [A] | $\eta_n$ [%] | $\cos\varphi_n$ |
|---|---|---|---|---|
| 1 | 23566 | 75,0 | 79,47 | 0,65 |
| 1,37 | 23538 | 77,8 | 83,40 | 0,61 |
| 1,92 | 23490 | 82,3 | 86,04 | 0,57 |
| 2,7 | 23411 | 88,8 | 86,87 | 0,53 |
| 3,76 | 23272 | 98,4 | 86,36 | 0,48 |

As seen in Fig. 6, efficiency keeps increasing as the outer air gap thickness increases up to 2,8 mm, reaching the maximum of 87,11 %. This confirms previous analytical findings. Fig. 7 clearly shows that the rotor losses are localized at the surface of the rotor because they mostly originate from the higher harmonics of the stator mmf. This harmonics are attenuated as the distance between the cup and the stator increases. As a consequence, rotor losses decrease.

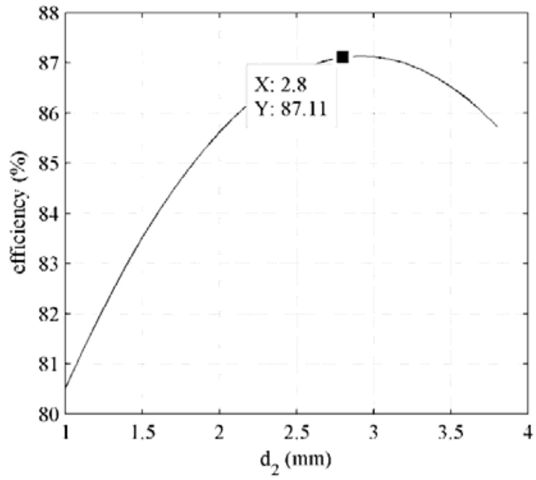


Figure 6. A curve that fits the values of rated coefficient of efficiency for different values of outer air-gap length

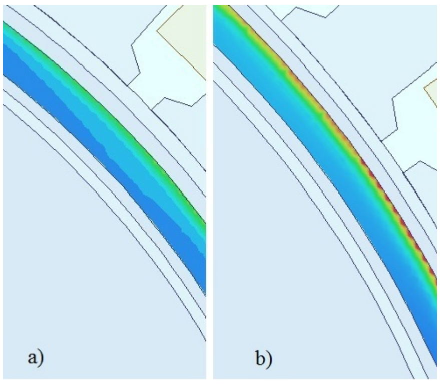


Figure 7. The total loss in the drag-cup rotor for two values of outer air gap length: a) $d_1$ = 1,37mm; b) $d_2$ = 1mm

Conducted optimization process yields the optimal values for drag-cup and air-gaps lengths which are summarized in Table VIII along with the main rated parameters of the optimal design. It can be seen from Table VIII that the optimal design has the efficiency that is close to the one predicted by the approximate analysis at the beginning of the design process. However, rated power factor is much lower than predicted. This is because the drag-cup motor has the inner air gap which does not exist in other high speed IM. It is interesting to note that relative value of no-load current is very close to the value predicted in the approximate analysis.

TABLE VIII. MAIN PARAMETERS OF OPTIMAL DESIGN

| Parameters | Values |
|---|---|
| $d_c$ [mm] | 1,8 |
| $d_1$ [mm] | 1 |
| $d_2$ [mm] | 2,8 |
| $\delta$ [mm] | 5,6 |
| $n_n$ [rpm] | 23395 |
| $I_n$ [A] | 89,8 |
| $i_0$ [%] | 70,67 |
| $\eta_n$ [%] | 87,11 |
| $cos\varphi_n$ | 0,52 |

## VI. Conclusion

Automotive systems represent an example in which high speed machines are commonly used. High speed machines must be highly optimized in order to have good efficiency and, at the same time, low mass and price. In this paper, stator of high speed drag-cup IM for automotive applications was dimensioned using basic analytical formulas, as well as taking into account some thermal and mechanical constraints. This motor is intended to be used in an auxiliary system of the vehicle such as KERS in Formula 1. The need for optimization process of cup thickness and air gaps lengths was shown by means of the detailed analytical analysis. In addition to this, the analysis that was conducted gave the approximate boundaries for these parameters along with prediction of no load current. It was shown then how this motor can be modeled in FEM software and how component of motor losses were calculated. Optimization process was then performed through series of simulations in FEM software with various cup thicknesses and air gaps lengths and for different motor speeds.

Optimization showed that increase of drag-cup thickness at first leads to the increase of motor efficiency due to the losses in cup decrease. Nevertheless, after a certain value of drag-cup thickness, motor efficiency starts to decrease because stator copper losses prevail due to increased total air gap which implies higher stator current. Increase of inner air gap results in decrease of efficiency because stator current and then stator losses grow and magnetic coupling between stator and rotor decreases so it was not in our scope to consider this phenomenon in FEM optimization process. Finally, it was shown that increase of outer air gap thickness enhances motor efficiency because drag-cup losses decrease due to attenuated higher harmonics of stator's mmf. Again, after a certain value of outer air gap length efficiency starts to decrease because negative consequences of increased total air gap prevail.

As the main result, optimal design is achieved with the best possible efficiency, which approves the conducted design and optimization process and shows that drag-cup motors can compete with other types of high speed induction machines if they are both carefully designed and optimized. Detailed optimization of the stator and rotor which takes into account mechanical and thermal phenomena will be the subject of future authors' work.

## References

[1] F. Mergiotti, F. Crescimbini, L. Solero, A. Lidozzi, "Design of a Turbo-Expander Driven Generator for Energy Recovery in Automotive Systems," in Proceedings of the 19th International Conference on Electrical Machines, Rome, 2010, doi: 10.1109/ICELMACH.2010.5607830

[2] F. Crescimbini, A. Lidozzi, L. Solero, "High-Speed Generator and Multilevel Converter for Energy Recovery in Automotive Systems," IEEE Trans. Industrial Electronics, Vol. 59, No. 6, June 2012, doi: 10.1109/TIE.2011.2160513

[3] T. Kawamura, H. Atarashi, T. Miyoshi, "Development of F1 KERS motor," in Proceedings of 25th World Battery, Hybrid and Fuel Cell Electric Vehicle Symposium and Exhibition, Shenzhen, China, November 5-9, 2010.

[4] B. Eberleh, T. Hartkopf, "A high speed induction machine with two speed transmission as drive for electric vehicles," in Proceedings of International Symposium on Power Electronics, Electrical Drives, Automation and Motion, Taormina, Italy, May 23rd – 26th, 2006. doi: 10.1109/SPEEDAM.2006.1649779

[5] W. L. Soong, G. B. Kliman, R. N. Johnson, R. A. White, J. E. Miller, “Novel High-Speed Induction Motor for a Commercial Centrifugal Compressor,” IEEE Trans. Industry Applications, vol. 36, No. 3, May/June 2000, doi: 10.1109/IAS.1999.799999

[6] K. V. Rodrigues, J. F. Pradurat, N. Barras, E. Thibaut, “Design of high-speed induction motors and associate inverter for direct drive of centrifugal machines,” in Proceedings of the 18th International Conference on Electrical Machines, Vilamoura, Algarve, Portugal, 2008, doi: 10.1109/ICELMACH.2008.4799870

[7] W. Fengxiang, Z. Wenpeng, Z. Ming, W. Baoguo, “Design Considerations of High-speed PM Generators for Micro Turbines,” in Proceedings of the International Conference on Power System Technology, Kunming, China, October 13-17, 2002, doi: 10.1109/ICPST.2002.1053524

[8] M. Centner, U. Schäfer, ”Optimized Design of High-Speed Induction Motors in Respect of the Electrical Steel Grade,” IEEE Trans. Industrial Electronics, Vol. 57, No. 1, January 2010, doi: 10.1109/TIE.2009.2029523

[9] M. Larsson, M. Johansson, L. Näslund, J. Hylander, “Design and evaluation of high-speed induction machine,” in Proceedings of the IEEE International Conference on Electric Machines and Drives, Madison, Wisconsin USA, June 1-4, 2003, doi: 10.1109/IEMDC.2003.1211245

[10] J. Pyrhönen, J. K. Nerg, P. T. Kurronen, U. Lauber, “High-Speed High-Output Solid-Rotor Induction-Motor Technology for Gas Compression,” IEEE Trans. Industrial Electronics, Vol. 57, No. 1, January 2010, doi: 10.1109/TIE.2009.2021595

[11] Y. Gessese, A. Binder, ”Axially Slitted, High-Speed Solid-Rotor Induction Motor Technology with Copper End-Rings,” in Proceedings of the International Conference on Electrical Machines and Systems, November 15-18, 2009, doi: 10.1109/ICEMS.2009.5382761

[12] A. Arkkio, T. Jokinen, E. Lantto, ”Induction and Permanent-Magnet Synchronous Machines for High-Speed Applications,” Proceedings of the 8th International Conference on Electrical Machines and Systems, Nanjing, China, September 27-29, 2005, doi: 10.1109/ICEMS.2005.202668

[13] H. Zhou, F-X. Wang, ”Comparative Study on High speed Induction Machine with Different Rotor Structures,” Proceeding of the International Conference on Electrical Machines and Systems, Seoul, Korea, October 8-11, 2007.

[14] M. Apstein, L. M. Blum, “Low-Inertia Induction Motors,” IEEE Trans. of the American Institute of Electrical Engineers, Power Apparatus and Systems, Part III., Vol. 76, Issue: 3 Page(s): 253 – 257, 1957, doi: 10.1109/AIEEPAS.1957.4499541

[15] R. Fillmore, ”Calculation or Eddy Current Paths in Drag-Cup Induction Motor Rotors,” IEEE Trans. of the American Institute of Electrical Engineers, Power Apparatus and Systems, Part III., Vol. 75, Issue: 3 Page(s): 922 – 926, January 1956, doi: 10.1109/AIEEPAS.1956.4499385

[16] O. Bottauscio, F. Casaro, M. Chiampi, S. Giors, C. Maccarrone, M. Zucca, ”High-Speed Drag-Cup Induction Motors for Turbo-Molecular Pump Applications,” IEEE Trans. on Magnetics, Vol. 42, No. 10, October 2006, doi: 10.1109/TMAG.2006.879446

[17] K. Yamazaki, A. Suzuki, M. Ohto, T. Takakura, “Harmonic Loss and Torque Analysis of High Speed Induction Motors,” IEEE Trans. Industry Applications, vol. 48, No. 3, Page(s): 933 – 941, May-June 2012, :doi: 10.1109/TIA.2012.2191252

[18] J. Lähteenmäki, “Design and Voltage Supply of High Speed Induction Machines,” Ph.D. dissertation, Acta Polytechnica Scandinavica, 2002.

[19] J. Pyrhönen, T.Jokinen, V.Hrabovcova. Design of rotating electrical machines. John Wiley & Sons, Ltd., 2008.

[20] J. F. Gieras. Advancements in Electric Machines. Springer, 2008.

[21] О. Гольберг, И. Свириденко. Проектирование электрических машин. Висшая школа, Москва, 2006.

[22] S. N. Vukosavic. Electrical Machines. Springer, 2013.

[23] K. Yamazaki, A. Suzuki, M. Ohto, T. Takakura, S. Nakagawa, “Harmonic Loss Analysis and Air-Gap Optimization of High Speed Induction Motors,” in Proceeding of the Energy Conversion Congress and Exposition, Page(s): 3963 – 3970, Atlanta, USA, 2010, doi: 10.1109/ECCE.2010.5617797

[24] Nikola Binchi. Electrical machine analysis using finite elements, Taylor & Francis, 2005.

[25] P. Beckley. Electrical steels for rotating machines. The Institution of Engineering and Technology, London, UK, 2002.

[26] Joao Pedro A. Bastos, Nelson Sadowski. Electromagnetic modeling by finite element methods, Taylor & Francis, 2003, pp. 435-448

[27] J. Saari, “Thermal analysis of high-speed induction machines,” Ph.D. dissertation, Acta Polytechnica Scandinavica, 1998.

[28] Y. Yamada, “Torque resistance of a flow between rotating co-axial cylinders hawing axial flow,” Bulleting of JCME, vol. 5, no. 20, pp. 634-642, 1962.